KMS Technologies – KJT Enterprises Inc.

Chapter 2
Basic Theoretical Background

extract from

Strack, K.-M., 1992, reprinted 1999
Exploration with deep transient electromagnetic: Elsevier, 373 pp.

Chapter 2
Basic Theoretical Background

The original theory of *transient electromagnetics* can be found in two textbooks (Vanyan,1967; Kaufman and Keller, 1983). Here, only the key equations will be given. The derivations of the equations are slightly different from the concepts in the above mentioned books, but give a more consistent picture suitable for todays numerical implementations. One exemplary derivation is given in appendix 1. We mainly follow the concepts by Weidelt (1985), and Ward and Hohmann (1988). A well described summary of all equations and the derivations can be found in Petry (1987) and Boerner (1992), and of the entire LOTEM system in Strack (1985). The general framework how to relate the derivations to controlled source electromagnetic techniques for petroleum exploration can be found in Nekut and Spies (1989).

After explaining the physical and of deep transient electromagnetics, emphasis is given to the different ways of presentation of the field data. The goal is to provide the reader with ways of relating the material in this chapter to standard geoelectric data presentation (apparent resistivities) and a more direct of the resistivity structure.

PHYSICAL PRINCIPLES

The deep transient electromagnetic method described in this book uses a grounded wire transmitter and receivers for the electric field and the time derivative of the magnetic field (figure 2.1). The transmitter dipole is usually several hundred meters to several kilometers long. The distance between transmitter and receiver site, called *offset*, varies between 2 and 20 km. Shorter or longer offsets are possible but are less often used. When the offset is approximately equal or larger than the exploration depth, the method is also called Long Offset Transient Electromagnetics (LOTEM).

A square wave current is injected into the ground through the transmitter bipole (following called dipole). The current switching induces electromagnetic induction currents in the subsurface. The diffusion process of the transient electromagnetic fields can be visualized using the *smoke ring concept* (Nabighian, 1979; Oristaglio and Hohmann, 1984; Gunderson et al, 1986). For a grounded wire transmitter which consists of a small bipole, one can calculate the electric field within a half-space shown in figure 2.2. The solid contour lines represent lines of equal electrical field strength corresponding to positive current flow, whereas the dashed ones represent negative current flows. The induction currents flow perpendicular to the plane of the drawing. Therefore, one can imagine the current flow extending out of the page at the top and

returning in the lower part of the frame. The individual frames in the figure represent snapshots at different times after current turn off, denoted on the lower right of the frames. At early times the currents are predominantly located near the transmitter wire. With increasing time the induction currents diffuse downwards.

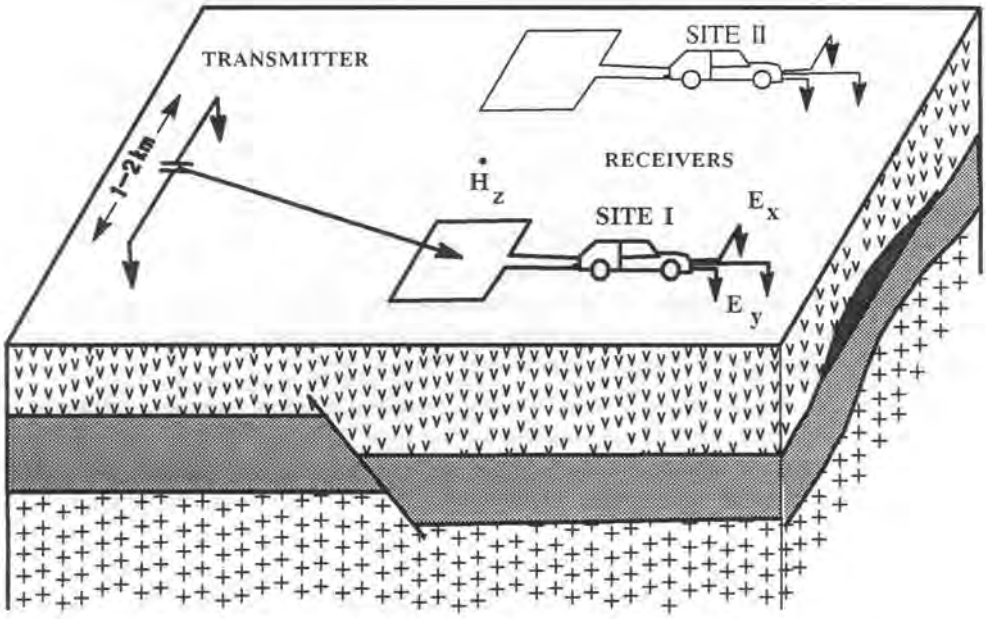

Fig. 2.1: Typical LOTEM transmitter and receiver setup (single site system).

If we now introduce an intermediate layer in the earth model, the diffusion patterns change. In figure 2.3 an additional layer of 2000 Ohm-m resistivity has been introduced at a depth of 3 kilometers. When the induced currents, which are flowing perpendicular to the plane of the drawing, reach the layer boundary, they start to diffuse outwards with increasing time. This causes the signal information at the receiver to come from an area of integration somewhere between the transmitter and receiver. Figure 2.4 gives a comparison of the diffusion process for a half-space and two-layer models for the 10 msec snapshot. The diffusion speed depends strongly on the resistivity of the subsurface. In the two-layer case a typical resistivity contrast for German crustal applications has been selected. The sharp corners in some of the contour lines are solely due to the resolution of the contouring.

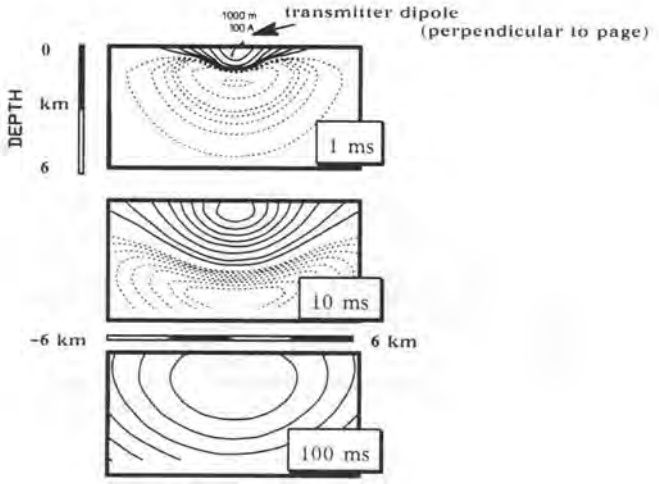

Fig. 2.2: *Smoke rings* for a grounded dipole in a half-space with 200 Ωm resistivity. The different frames mark different times after current turn off. The contours represent lines of equal electric field strength. The dashed lines mark opposite polarity.

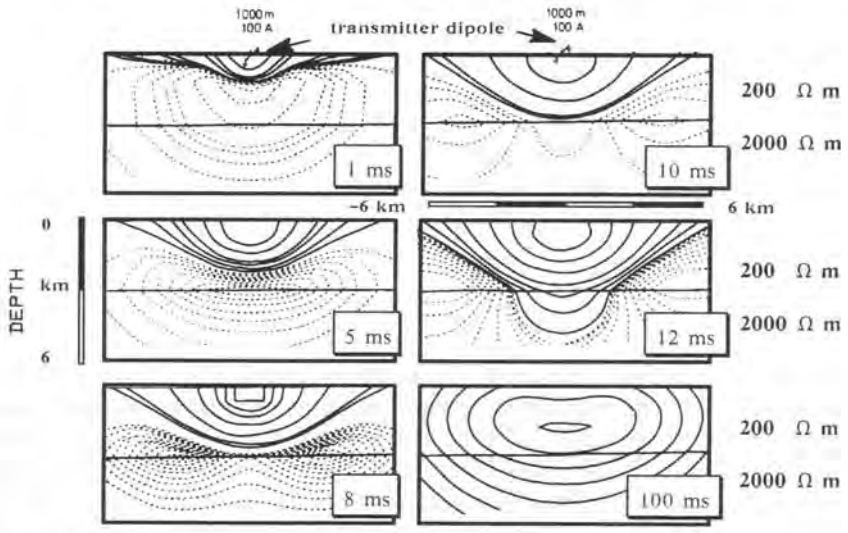

Fig. 2.3: System of *smoke rings* for a grounded wire dipole on a two-layer earth model. The contours represent lines of equal electric field strength. The dashed lines mark opposite polarity.

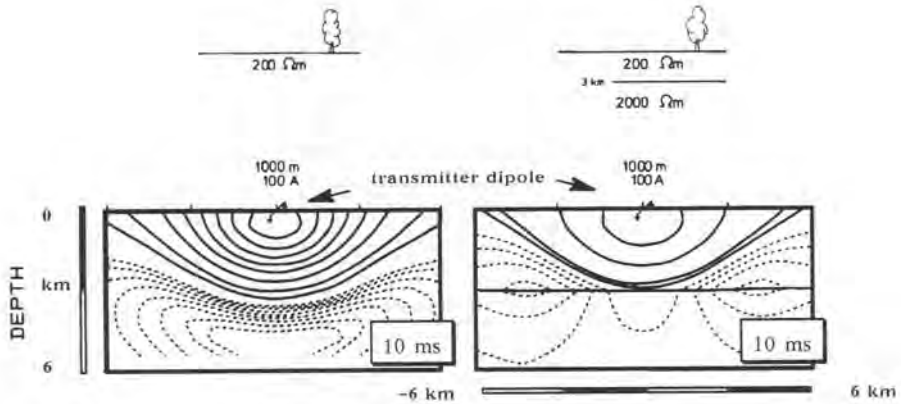

Fig. 2.4: Comparison of the diffusion process of induction currents 10 ms after current turn off for a half-space and a two-layer earth model.

THEORETICAL BACKGROUND

The derivation of the electromagnetic field equations is based upon the quasi-stationary Maxwell's equations:

$$\begin{aligned} \text{rot } \mathbf{E} &= -\delta\mathbf{B} / \delta t && \text{(Faraday's law)} \\ \text{rot } \mathbf{H} &= \mathbf{j} && \text{(Ampere's law)} \\ \text{div } \mathbf{D} &= 0 && \text{(Coulomb's law)} \\ \text{div } \mathbf{B} &= 0 \\ \mathbf{j} &= \sigma\mathbf{E} \\ \mathbf{B} &= \mu\mathbf{H} \\ \mathbf{D} &= \epsilon\mathbf{E} \end{aligned} \qquad (2.1)$$

where ϵ is the dielectric constant of vacuum permeability ($\mu = \mu_0 = 4\pi\ 10^{-7}$ Vs/Am), **E** is the electric field intensity, **D** the electric displacement, **B** the magnetic induction, t the time, **H** the magnetic field, **j** the current density, σ the electrical conductivity. Using scalar potentials (Weidelt, 1985; Petry, 1987; Ward and Hohmann, 1988; Boerner and West, 1989) the Maxwell's equations can be solved for a layered earth. The selected scalar potentials are commonly denoted Φ_E and Φ_M. They satisfy the above equations independently. In potential theory these scalar potentials are sometimes called Debye potentials or poloidal and toroidal potentials. Φ_E does not generate an electric field component in vertical direction and Φ_M does not generate a magnetic component in vertical direction. Thus Φ_E is also called transverse or tangential electric

(TE) mode and ϕ_M is called transverse or tangential magnetic (TM) mode. Often the word polarization is used equivalent to mode.

In the 1-D case the TE mode contains only horizontal and the TM mode vertical currents. The following equations are for the voltages measured by induction loop magnetometers, U, or electric field sensors, V:

$$U_z(\mathbf{r}, t) = \frac{-1}{2\pi} \int_{-\infty}^{\infty} \mu_0 A e^{i\omega t} \frac{D_0 \cos\phi}{4\pi} \int_0^{\infty} \frac{B_{E1}(\kappa,\omega) - \kappa}{B_{E1}(\kappa,\omega) + \kappa} \kappa J_1(\kappa r)\, d\kappa d\omega \tag{2.2}$$

$$V_x = l\, E_x(\mathbf{r}, t) = \frac{-l}{2\pi i} \int_{-\infty}^{\infty} \frac{e^{i\omega t}}{\omega} \frac{-i\omega\mu_0 D_0}{4\pi} \int_0^{\infty} \left\{ \left(\frac{B_{H1}(\kappa,\omega) - \kappa}{\alpha^2} - \frac{1}{B_{E1}(\kappa,\omega) + \kappa} \right) \right.$$

$$\left(\frac{2}{r} J_1(\kappa r) \left(2\cos^2\phi - 1 \right) - 2\kappa J_0(\kappa r) \cos^2\phi \right)$$

$$\left. + \frac{B_{E1}(\kappa,\omega) - \kappa}{B_{E1}(\kappa,\omega) + \kappa} K J_0(\kappa, r) \right\} d\kappa d\omega + \frac{\rho_1 D_0}{2\pi r^3} \left(2 - 3\sin^2\phi \right) \tag{2.3}$$

where U_z is the voltage induced in an induction coil with the area A. ϕ is the angle between the x-coordinate (parallel to the transmitter dipole) and the offset vector **r**, y is the coordinate perpendicular to the dipole, ω is the angular frequency, κ is the wave number, J_0 and J_1 are Bessel functions, V_x and V_y are the voltages measured with an electric field sensor of the length *l*, D_0 is the transmitter dipole moment. B_{E1} and B_{H1} are the reciprocal modified impedances at the surface whichare defined as:

$$B_{En,Hn} = \alpha_n \qquad \alpha_m^2 := \kappa^2 + i\omega\mu_0\sigma_m$$

$$B_{Em} = \alpha_m \frac{B_{Em+1} + \alpha_m \tanh(\alpha_m d_m)}{\alpha_m + B_{Em+1} \tanh(\alpha_m d_m)} \tag{2.5}$$

$$B_{Hm} = \alpha_m \frac{B_{Hm+1} + \alpha_m \beta_m \tanh(\alpha_m d_m)}{\alpha_m \beta_m + B_{Hm+1} \tanh(\alpha_m d_m)} \tag{2.6}$$

$$m = M-1, \ldots, 1 \qquad d_m = h_{m+1} - h_m \qquad \beta_m = \sigma_{m+1} / \sigma_m$$

where n is the number of layers and h_i their respective thicknesses. The recursion is defined such that it starts with the lowest layer, the bottom half-space. There the electromagnetic field disappears at infinity which allows its solution. From this n-th layer one works upwards to the (n-1)-th layer until the surface is reached. With these formulae the voltages for a layered earth model can be calculated and compared with the voltages received in the field.

One of the frequently asked questions is why there are no direct electromagnetic reflections when the equation can be nicely expressed as recursion formula for the individual layers. The cause lies in the neglect of the displacement currents which reduce the wave equation to a diffusion equation. To show that the latter can be neglected, we use the wave equations for the electric and magnetic fields:

$$\nabla^2 \mathbf{E} + (\mu \epsilon \omega^2 - i \mu \sigma \omega) \mathbf{E} = 0 \qquad (2.7)$$

and

$$\nabla^2 \mathbf{H} + (\mu \epsilon \omega^2 - i \mu \sigma \omega) \mathbf{H} = 0. \qquad (2.8)$$

The bracket can be reduced to $(- i \mu \sigma \omega)$ when the first term is very small or $1 / \epsilon \omega \rho \gg 1$. For most rocks the dielectric constant ϵ is in the order of 10^{-10} As/Vm. For resistivities around 1 to 10000 Ωm and frequency below 1kHz the quantitiy $1 / \rho \omega \epsilon = 1 / (10^4 \cdot 10^3 \cdot 10^{-10}) = 10^3 \gg 1$. This means the displacement current can be neglected indeed.

The above theory is sufficient for the inversion, but leaves the operator with no feeling for the data and their correspondence to the geology. Thus we need to find a way of presenting the data for the operator in the field. We borrow from other electrical methods the concept of apparent resistivity to do this.

APPARENT RESISTIVITY

One definition of apparent resistivity is given by Sheriff (1984):

"The resistivity of homogeneous isotropic ground which would give the same voltage – current relationship as measured."

With this, apparent resistivities have been defined for all electrical and electromagnetic methods. All of them have as their goal to define the physical change of the

subsurface as a function of a parameter specific to the method. In DC-resistivity soundings, the spacing can be used to obtain an estimate about the exploration depth. For frequency domain methods (magnetotellurics, audio magnetotellurics, controlled source audio magnetotellurics, frequency domain soundings and others), the apparent resistivity and phase curves are related to frequency which is connected directly via the skin depth to the exploration depth. For transient EM methods the time window is directly related to the exploration depth range (Spies, 1989). The distance between transmitter and receiver, called offset, is the governing factor at which time window conductivity features in the subsurface are resolvable by an instrument with a given dynamic range. The resolution of these features strongly depends upon the signal-to-noise ratios obtained in the survey area. In electrical/electromagnetic methods, one standard procedure is used to derive the apparent resistivity formulae. The goal of this procedure is to relate the apparent resistivity to the resistivity of a half-space. The resulting equations are to be manipulated only with the knowledge of the field parameters (voltages, array dimension, current, frequency, time etc.) until an apparent resistivity formula can be found. The general steps are:

- Derive the equation for a half-space voltage as a function of the half-space resistivity.
- Rewrite this equation to show the half-space resistivity as a function of the measured voltage, U_m.
- Normalize the measured voltage and relate it to the half-space voltage, i.e.

$$\frac{\rho_a}{\rho^{HS}} = \frac{U_m}{U^{HS}} \tag{2.9}$$

- Leave the unknown, wanted quantity ρ_a on one side of the equation and adjust the equation such that the unknown resistivity of the half-space will cancel out.

Usually, additional constraints from physics help in carrying out the third and fourth steps. For DC-resistivity methods it means that for very long spacings the apparent resistivity approaches the resistivity of the bottom half-space. Similarly, for frequency domain methods, the high and low frequencies yield the true resistivities of the uppermost and deepest half-space. For time domain methods the very early time apparent resistivity gives the top layer and the late time apparent resistivity the bottom layer.

Following this procedure, the apparent resistivity formula can be used to correlate the earth response with the true resistivity changes in the subsurface. For LOTEM the derivation is slightly more complicated, since the half-space voltage depends in a nonlinear fashion on the half-space resistivity, namely:

$$V(t) = \frac{3\, D_0\, A\rho\, y}{2\, \pi\, r^5} \left[\operatorname{erf}\left(\frac{u}{\sqrt{2}} \right) - \sqrt{\frac{2}{\pi}}\; u \left(1 + \frac{u^2}{3} \right) e^{-u^2/2} \right] \tag{2.10}$$

with $u = \dfrac{2\pi r}{\tau}$ $\qquad \tau^2 = \dfrac{8\pi^2 \rho t}{\mu_0}$

and *erf* as the error function (Abramowitz and Stegun, 1964), V (t, ρ) is uniquely computable, whereas ρ (t, V) is not. There are times when a solution can be found. We thus need to consider the time limits of the above equation. For $t \to 0$, $u \to \infty$ and

$$\lim_{u \to \infty} \operatorname{erf}\left(\frac{u}{\sqrt{2}}\right) = 1 \quad \text{which yields} \tag{2.11}$$

$$U_{ET}^{HS} = \lim_{t \to 0} U(t) = \frac{3 D_0 Ay \rho}{2\pi r^5} \tag{2.12}$$

For $\tau \to \infty$ we obtain similarily:

$$U_{LT}^{HS} = \lim_{\tau \to \infty} U(t) = \frac{D_0 Ay}{40\pi\sqrt{\pi}} \frac{\mu_0^{5/2}}{\rho^{3/2} t^{5/2}} \tag{2.13}$$

where the subscript ET and LT indicate the early time ($t \to 0$) and the late time ($t \to \infty$), respectively. The early time equation is only valid for $\tau/r \leq 2$ and the late time equation for $\tau/r \gg 16$. Using the above and the rule for deriving the apparent resistivity formula we can define early and late time apparent resistivities as:

$$\frac{\rho_a^{ET}}{\rho_1} = \frac{U(t)_m}{U(t)_{ET}^{HS}} \quad \text{or} \quad \rho_a^{ET} = \frac{2\pi r^5}{3 D_0 Ay} U(t)_m \tag{2.14}$$

$$\frac{\rho_a^{LT}}{\rho_1} = \left(\frac{U(t)_{LT}^{HS}}{U(t)_m}\right)^{2/3} \quad \text{or} \quad \rho_a^{LT} = \left(\frac{D_0 Ay}{40\pi\sqrt{\pi}\, U(t)_m}\right)^{2/3} \left(\frac{\mu_0}{t}\right)^{5/3} \tag{2.15}$$

where ρ_a^{ET} = early time apparent resistivity

ρ_1 = resistivity of the half-space

i.e. $\rho_a \begin{cases} = \rho_1 & \text{for early times } \rho \text{ approaches the 1st layer resistivity} \\ = \rho_n & \text{for very late times } \rho \text{ approaches the last layer resistivity} \end{cases}$

ρ_a^{LT} = late time apparent resistivity

$U(t)_m$ = measured voltage

$U(t)^{HS}_{ET}$ = early time half-space voltage

$U(t)^{HS}_{LT}$ = late time half-space voltage

An example of half-space early and late time apparent resistivity curves is given in figure 2.5. Immediately after current switching, the early time apparent resistivity of the half-space is identical to the true resistivity of the medium. From the vertical marker when $\tau/r \leq 2$ at 0.6 seconds to approximately 30 seconds the apparent resistivity curve does not reflect the true subsurface resistivity (intermediate times). From

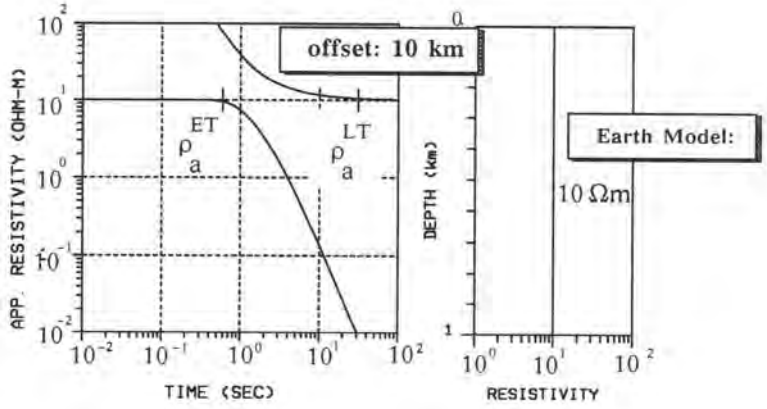

Fig. 2.5: Example of an early and late time apparent resistivity curve for a homogenous half-space with 10 Ωm resistivity.

30 seconds on we reach the so called late times when $\tau/r \gg 16$ and the apparent resistivity curve reflects the true earth resistivity again. Figure 2.6 shows the apparent resistivity curves for a three-layered earth. We can see an increase in the apparent resistivity curve at early times caused by the more resistive second layer. It then decreases again because it looses its validity and only reflects the decay of the physical electromagnetic field. The late time apparent resistivity curve, on the other hand, asymptodes to a value representative of the lowest (semi-infinite) layer.

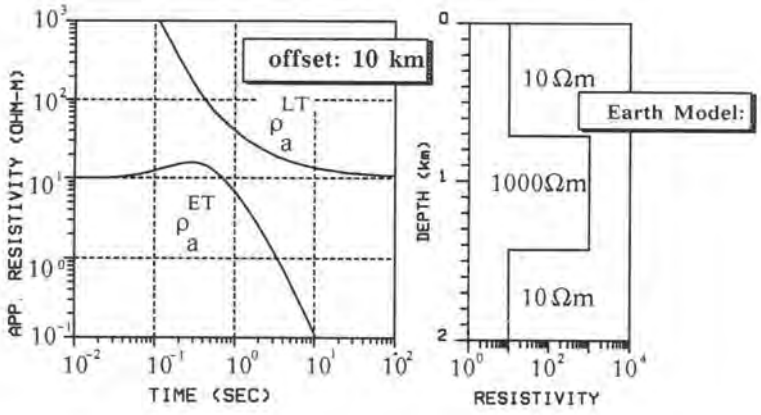

Fig. 2.6: Example of an early and late time apparent resistivity curve for a three–layer earth model with the second layer being highly resistive.

Following this formalism (Petry, 1987) one can derive the apparent resistivity formulae for the different electromagnetic field components which are usually measured in the field:

for the time derivative of the vertical magnetic field:

$$\rho_{a,z}^{ET}(t) = \frac{2\pi r^5}{3 A D_0 y} U_z(t) \tag{2.16}$$

$$\rho_{a,z}^{LT}(t) = \left(\frac{A D_0 y}{40\pi\sqrt{\pi}\, U_z(t)} \right)^{2/3} \cdot \left(\frac{\mu_0}{t} \right)^{5/3} \tag{2.17}$$

for the electric field parallel to the wire (Ex):

$$\rho_a^{ET}(t) = \frac{4\pi r^3 E_x}{3 D_0 \sin^2\phi} \tag{2.18}$$

$$\rho_a^{LT}(t) = \frac{-2\pi r^3 E_x}{D_0 \left(1 - \frac{3}{2}\sin^2\phi\right)} \tag{2.19}$$

and for the electric field perpendicular to the wire (E_y):

$$\rho_a^{ET}(t) = \frac{-4\pi r^3 E_y}{3 D_0 \cos\phi \sin\phi} \tag{2.20}$$

$$\rho_a^{LT}(t) = \frac{-4\pi r^3 E_y}{3 D_0 \cos\phi \sin\phi} \tag{2.21}$$

When carrying out LOTEM measurements, one has to overcome the electromagnetic noise in the survey area. Usually, this means that analog filters are used during the recording of the data. When converting the data to apparent resistivities, the curves look different from the curves in figures 2.5 and 2.6. The curves usually have a steep slope at early times. This slope is caused by the system response, which will be explained in the next chapter. Because the data contains the system response, these curves are called *resistivity transforms* rather than apparent resistivities. Figure 2.7 shows an example of the *resistivity transforms* for the earth models from figure 2.5 and 2.6.

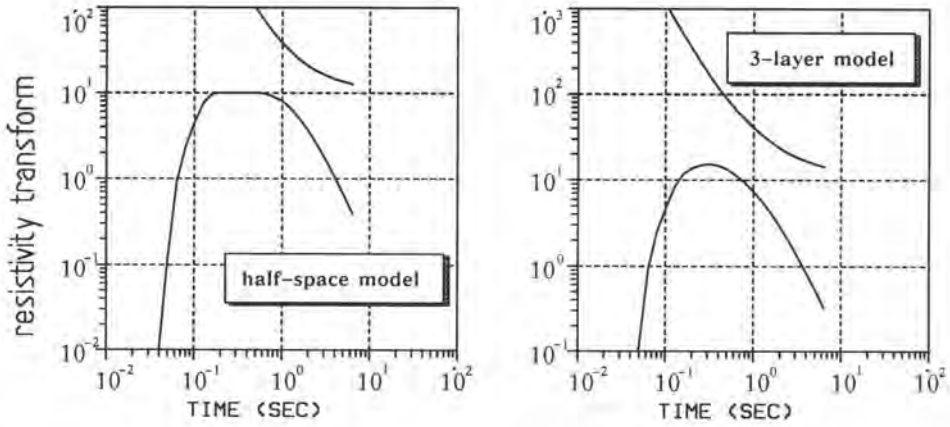

Fig. 2.7: *Resistivity transforms* for the models from figure 2.5 (left) and 2.6 (right).

At this point, a warning about the use of apparent resistivities for LOTEM seems appropriate. They show only one way of normalizing the data for a first quick look at the field results. Because of the complicated field behaviour and imperfections in the data acquisition (system response and noise) it is difficult to derive a reliable earth model directly from the apparent resistivity curves. Actually, the apparent resistivities have very little meaning for the electric fields and we thus always use the voltages and invert strictly on voltages which are, as already mentioned above, a very good way of

accurately evaluating the data. There have been several attempts without much success to derive an apparent resistivity formula valid for all times for LOTEM (Yang, 1986; Spies and Eggers, 1986; Strack, 1987). They are summarized in the following for completeness.

ALL TIME APPARENT RESISTIVITY

Although the usefulness of apparent resistivity curves for interpretation purposes is debatable, they can help to compare field data from different receiver sites and to obtain some form of normalized data set for contouring and imaging.

Because the increasing number of data sets requires a fast way of data presentation, the quest for an all time apparent resistivity is becoming more important. In the literature only one paper for LOTEM *all time apparent resistivity* (Yang, 1986) is readily available. Yang extended the *all time resistivity* concept and derived a formulation for some specific cases. Similar earlier semi-successful attempts were carried out by Stoyer and Strack (Strack, 1985). All of them have in common that they use the voltage curve as basis for all time apparent resistivity formulation. Spies and Eggers (1986) mention a more promising route using the magnetic field values as basis. They applied their concept only to in-loop TEM data. Karlik (Karlik and Strack, 1990) applied it to LOTEM data.

The first attempt was made by Stoyer in 1981 as a time dependent interpolation between the early and the late time curves. The results for a two-layer model are shown in figure 2.8. For a half-space the true resistivity is obtained. When the second layer is less resistive, the apparent resistivity approaches the value of the second layer

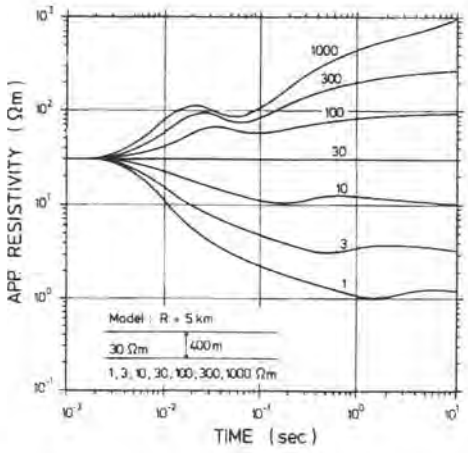

Fig. 2.8: *All time apparent resistivity curves* by Stoyer for a two-layer model (after Strack, 1985).

and then undershoots before reapproaching it again. For a more resistive second layer it first undershoots and then approaches the resistivity of the second layer. Since the undershoots do not always appear at the same time window, it is very difficult for the interpreter to recognize them without attributing them to an additional layer.

Strack (1985) used a least squares technique to avoid some of the additional flexures. When an additional flexure was automatically recognized as such, a flat part in the apparent resistivity curve resulted. However, even for a four-layer model, additional flexure in the curve could not be completely avoided. In figure 2.9 the curve for a 1500 m thick third conductive layer exhibits the part where no solution could be found between 0.6 to approximately 2 seconds. If this layer is only 1000 m thick the *all time apparent resistivity* curve is smooth but reflects a typical five-layer apparent resistivity curve.

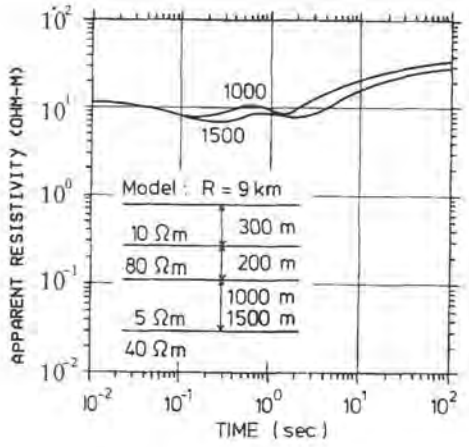

Fig. 2.9: *All time apparent resistivity curves* for a four-layer model using Strack's least square formulation (after Strack, 1985).

Yang (1986) conditioned the least squares process further and obtained a larger class of all time apparent resistivity curves without significant flexures. However, he could not obtain curves for all classes of models, in particular, not for realistic long offsets. Only slight additional flexure is visible in his three-layer curves. It is difficult to decide which one of these flexures is due to real geology or due to the algorithm. Since Yang used mainly offsets smaller than four times the dipole length, the applicability of his approach for LOTEM data is limited.

Karlik (Karlik and Strack, 1990) used the idea described by Spies and Eggers (1986) which uses the magnetic field instead of its derivative. This is achieved by integrating the voltage response. The measured data set (as a function of transmitter to receiver offset) is compared with the magnetic field of a homogenous half-space for which the conductivity is to be found such that:

$$H_z^m = H_z^{HS} \quad \text{or} \quad H_z^m - H_z^{HS} = 0$$

or in general terms:

$$g - f(\rho) = 0 \tag{2.22}$$

From this equation, one can obtain ρ using

$$\rho = f^{-1}(g) \tag{2.23}$$

Equation 2.23 can only be solved numerically using a technique such as the Newton–Raphson method. The initial resistivity of the homogenous half-space is varied until equation 2.22 is satisfied. Using this procedure and the magnetic field rather than the voltage response avoids the problem of the non-single valued function described in

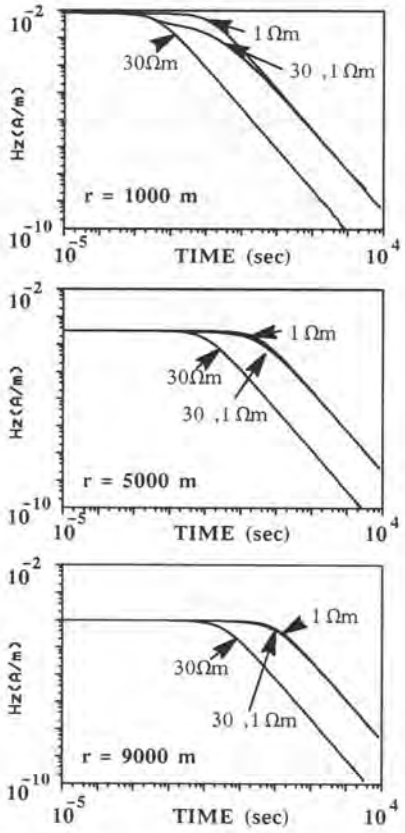

Fig. 2.10: Magnetic fields for two half-spaces with the resistivities of 30 Ωm and 1 Ωm and for a two-layer model with the same resistivities (30 Ωm, 1 Ωm; first layer thickness = 400 m) for offsets of 1 km, 5 km and 9 km.

equation 2.10 for the voltage response. Figure 2.10 shows the magnetic field response for two half-spaces with different resistivities and a two-layer model with the two respective half-spaces resistivities. The magnetic field for the two-layer model follows first the upper layer resistivitiy and then approaches the curve of the resistivity of the second layer. The magnetic field is a monotonic function which allows the calculation of its inverse. The result is the resistivity ρ as a function of the magnetic field. Only slight deviations from the shape of the half-space magnetic field are obtained for different offsets. These deviations are strongest for the upper layer when close to the transmitter, as can be seen in figure 2.11.

Figure 2.11 shows a suite of three-layer *all time apparent resistivity* curves with varying second layer resistivity. The curves are well behaved and do not show the additional flexure as shown above.

Note that no undershoot or overshoots exist as usually for frequency domain curves (Spies and Eggers, 1986).

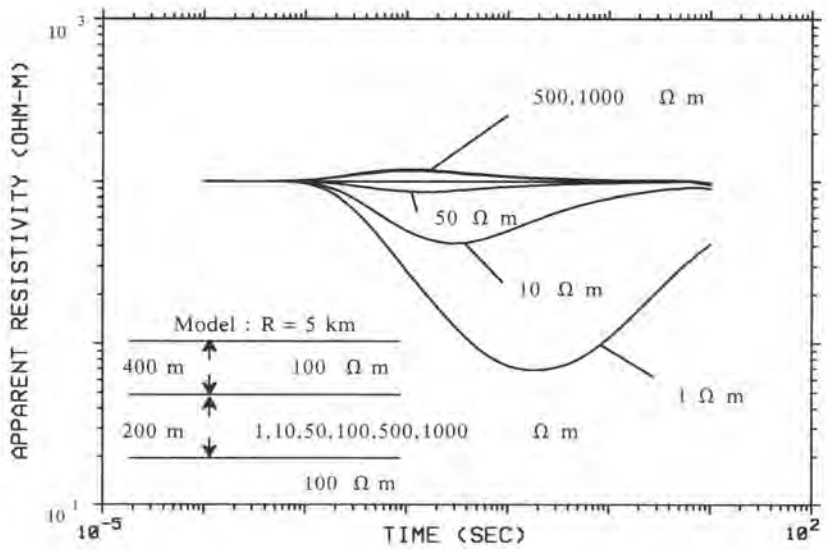

Fig. 2.11: *All time apparent resistivity curves* for a three-layer model with varying second layer resistivity (after Karlik and Strack, 1990).

Figure 2.12 shows the results using the *all time apparent resistivity* formulation for the same model as used by Yang (1986). It is clear that all time apparent resistivity does not show the flexures as exhibited in Yang's approach.

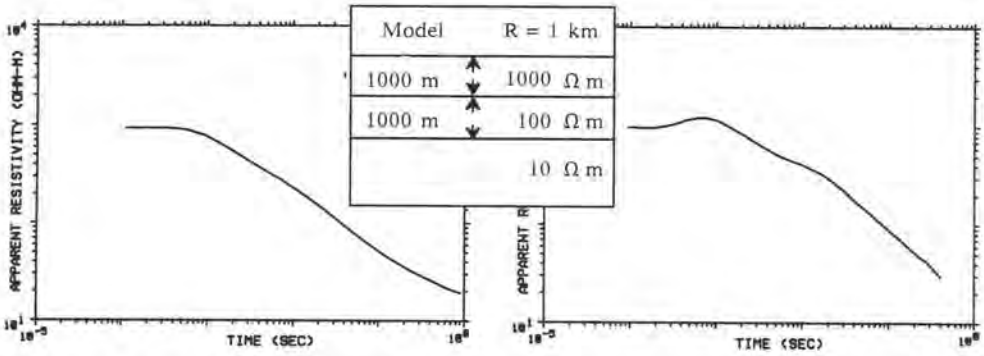

Fig. 2.12: *All time apparent resistivity curves* for the three-layer model used by Yang (see figure 2.10) (Karlik and Strack, 1990). Left is the *all time apparent resistivity* curve derived from the magnetic field and on the right the corresponding curve by Yang. Both curves are calculated for an offset of 1 km.

Figure 2.13 shows the *all time apparent resistivity curves* for the four-layer model used by Strack (1985). Again no additional flexures are visible and the curves are well behaved.

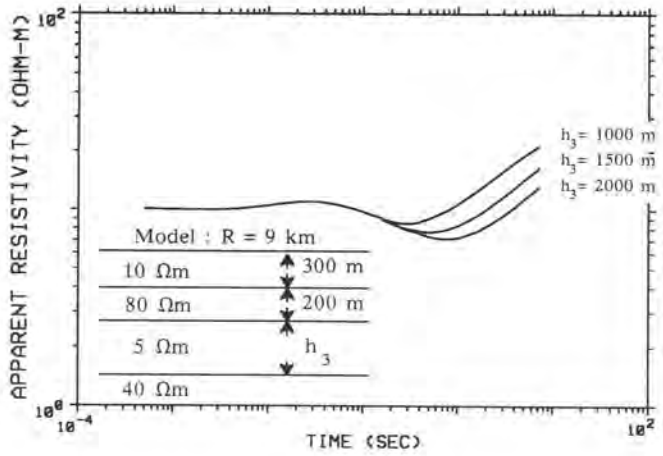

Fig.2.13: *All time apparent resistivity curves* for a four-layer model used for figure 2.9 (after Karlik and Strack, 1990).

The above calculations were done with synthetic data. Applying this procedure to real data one generally faces two problems:

- The data is influenced at early times by the system response and is thus distorted.

- At later time the noise prevails and causes additional numerical errors.

Therefore, the *all time* algorithm should be only applied to deconvolved data – that is data after removal of the system response. Figure 2.14 shows an example of a field data set. The left side of the figure shows the conventional early and late time apparent resistivity curves with the 95% confidence envelopes. The right graph shows the respective *all time* curve derived from the field data. For better visualization the data has been displayed without error bars. The arrow marks the location where the all time curve is no longer reliable and the error prevails. This is very difficult to recognize from the all time curve alone.

The advantage of having the all time curve lies in the capability of generating less biased pseudo-sections and image sections which were otherwise misrepresented by the early and late time approximation.

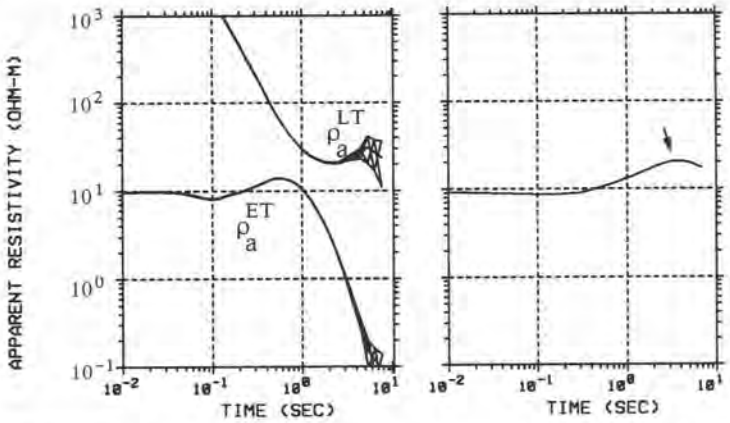

Fig. 2.14: Field data of an early and late time apparent resistivity curves (left) and the respective *all time apparent resistivity curve* (after Karlík and Strack, 1990).

IMAGE PRESENTATION OF THE DATA

The conversion of electromagnetic data to a direct subsurface image has been investigated by many researchers. The goal is the conversion of the measurements to a subsurface image which approximates the geology. Significant work was done in the Soviet Union (i.e. Zhdanov and Matusevich, 1984) with the concept of migrating the EM fields similar to seismics. Some of the early work of interpreting electromagnetic data by transformation to interval resistivities was done by Kamenetsky (Kamenetsky 1985; Kamenetsky and Porstendorfer, 1983). In the western world many papers concerning the direct presentation of transient EM data appeared in the literature (Nabighian, 1979; Barnett, 1984; Raiche and Gallagher, 1985; Spies and Eggers 1986; Polzer, 1986; Nekut 1987; Macnae and Lamontagne 1987; Fullagar, 1989; Eaton and Hohman, 1989; Macnae et al, 1991; Smith and Buselli, 1991). All these techniques

have the advantages and drawbacks. The reason lies in the different field behaviors for different field layouts and also for the large range of resistivity contrasts. For details on the different methods, the reader is referred to the above mentioned articles. Here two different approaches are described. The first approach goes via a simple transformation from the data directly the resistivity/conductivity image. The second approach uses a model assumption and compares the measured data with the model response until a satisfactory fit is obtained.

The first approach is based on the all time apparent resistivity curve. The goal is to find a transformation such that this curve is converted to a resistivity versus depth curve. As all time apparent resistivity curve one should preferably use the all time curve derived through the magnetic field conversion as described above. This curve is used to calculate the diffusion velocity and with the diffusion velocity a diffusion depth. From the diffusion depth and the total conductance of all strata above this depth one can calculate an image conductivity. The diffusion velocity is obtained using the formula given by Macnae and Lamontagne (1987) for the slowness, the inverse of the velocity;

$$v_d(t) = \sqrt{\frac{\rho_a(t)}{\mu_0 \, 2t}} \qquad (2.24)$$

where $v_d(t)$ is the diffusion velocity and $\rho_a(t)$ the all time apparent resistivity The factor 1/2 inside the square root is different for the different authors and depends on how they express the depth of penetration. We found the above expression by Macnae and Lamontagne (1987) to be the best fitting one for LOTEM data. The diffusion depth is then:

$$z(t) = \int_0^t v(t)\, dt' \qquad (2.25)$$

Knowing the diffusion depth for every time, we assume that the apparent resistivity is :

$$\rho_a(t) = \frac{Z_d(t)}{S_d(Z(t))} \qquad (2.26)$$

which $S_d(Z(t))$ is the total conductance of the strata above a specific time and diffusion depth. Subscript d denotes the respective values using the diffusion depth. The image conductivity (inverse resistivity) in a depth interval dz is the change of the conductance with depth or:

$$\sigma_i = \frac{1}{\rho_i} = \frac{dS}{dz_d} = \frac{d(z/\rho_a)}{dz_d} \qquad (2.27)$$

Because this conductivity is the conductivity between depth intervals it is termed *interval conductivity* / or *interval resistivity*. Figure 2.17 (below) shows an example of the *interval conductivity* in comparison with the *source image conductivity* and is discussed below.

The second approach follows closely the approach of Eaton and Hohman (1989). The derivation is explained in more detail because it gives fast subsurface images for LOTEM. The technique proposed by Eaton and Hohman uses a single image which varies in position with time while Macnae and Lamontagne (1987) use multiple images. The basis for the imaging technique is the comparison of the magnetic field of the image current with the measured earth response converted to magnetic field values. The image is located underneath the transmitter with identical dipole moment. It is thus called *source image* or *current image*. Its depth as function of time is defined via the maximum of the electric field inside a homogeneous half-space. As for equation 2.10 we obtain for the electric field underneath the transmitter:

$$E_x(z,t) = \frac{D_0\,\rho}{\pi\, z^3}\left[\operatorname{erf}\left(\frac{u}{\sqrt{2}}\right) - \frac{1}{2} + \left(\sqrt{\frac{2}{\pi}}\;u - \frac{1}{2}\right)\left(1+\frac{u^2}{2}\right) e^{-u^2/2}\right] \quad (2.28)$$

The time of maximum of E_x for a given depth is obtained by calculating the first derivative of E_x with respect to time

$$\left.\frac{dE_x(z,t)}{dt}\right|_{z = z_{image}} = 0 \quad (2.29)$$

From this, the image depth is calculated:

$$z^2(t)_{image} = \frac{4t}{\mu_0\,\sigma} \quad (2.30)$$

The magnetic field at the receiver site from a current filament located at this depth is according to Biot-Savart's law:

$$H_z = \frac{I}{4\pi}\;\frac{y}{y^2+z^2}\;\frac{x+l}{((x+l)^2+y^2+z^2)^{1/2}}\;\frac{x-l}{((x-l)^2+y^2+z^2)^{1/2}} \quad (2.31)$$

where l is half of the transmitter dipole length dl; z is the image depth. From the above equation z(t) is determined by iteratively fitting the image magnetic field to the measured or calculated one.

We now have the magnetic field from a current filament (*source image*) at the receiver site and the image depth as a function of conductivity. From equation 2.30, we

can calculate a slowness:

$$\frac{dt}{dz} = \frac{1}{2} z \mu_0 \sigma \tag{2.32}$$

Building the second derivative with respect to z yields the conductivity of the image:

$$\sigma = \frac{2}{\mu_0} \frac{d^2 t}{dz^2} \tag{2.33}$$

This expression is similar to the ones derived by Eaton and Hohmann (1989) and Macnae and Lamontagne (1987).

The computation of the *source image* can be split in three steps. First, the conversion of the field data (deconvolved) or synthetic data to magnetic field values. Second, the calculation of the image depth by fitting the image magnetic field to the measured one. Third, the calculation of the image conductivity. When calculating the magnetic field no major problems occur except when the field data becomes very noisy. The image depth values are obtained for given time values for a guess half-space resistivity. In practice, the all time apparent resistivity is calculated and its inverse used as input to calculate iteratively the image depth. If the guess half-space resistivity does not represent the average underlying earth model, the fit between the magnetic fields will not be good for all times. In this case, one should select a more appropriate half-space resistivity. Depending on how the procedures implemented, scale factors for the image depth and image conductivity must be derived by comparison with synthetic curves.

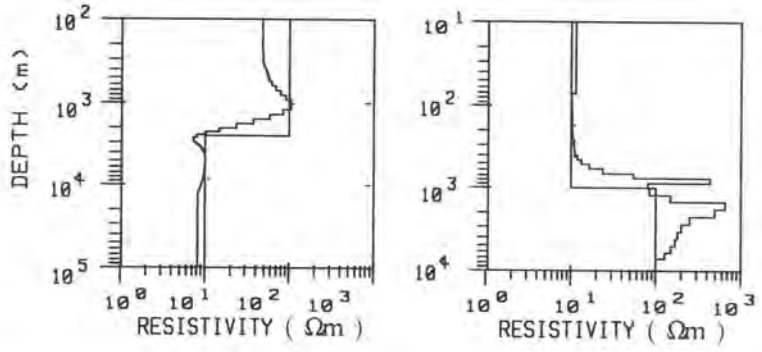

Fig. 2.15: *Source image* for a two-layer model.

The *source image* can be tested using synthetic data for a two-layer model as shown in figure 2.15 and a three-layer model displayed in figure 2.16. When the model

resistivity in figure 2.15 goes from a more resistive to a less resistive medium, only a small undershoot appears. When the resistivity increases sharply a large overshoot occurs. This overshoot has been observed by most authors and was the motivation for Smith et al (1991) to develop the spiked conductivity imaging. For figure 2.16, typical H, K, Q, and A-type three-layer models were selected. The Q-type (decreasing resistivty with depth) and the A-type model (increasing resistivity with depth) are reasonably well represented. For the H-type model (intermediate conductive layer), the conductive layer is well represented, but an overshoot occurs when reaching the boundary to the more resistive layer. For the K-type model (intermediate resistive layer), the *source image* is broadened over a large depth range. When considering that the source image is a fast - almost real time - initial guess, it represents the resistivity structure reasonably well.

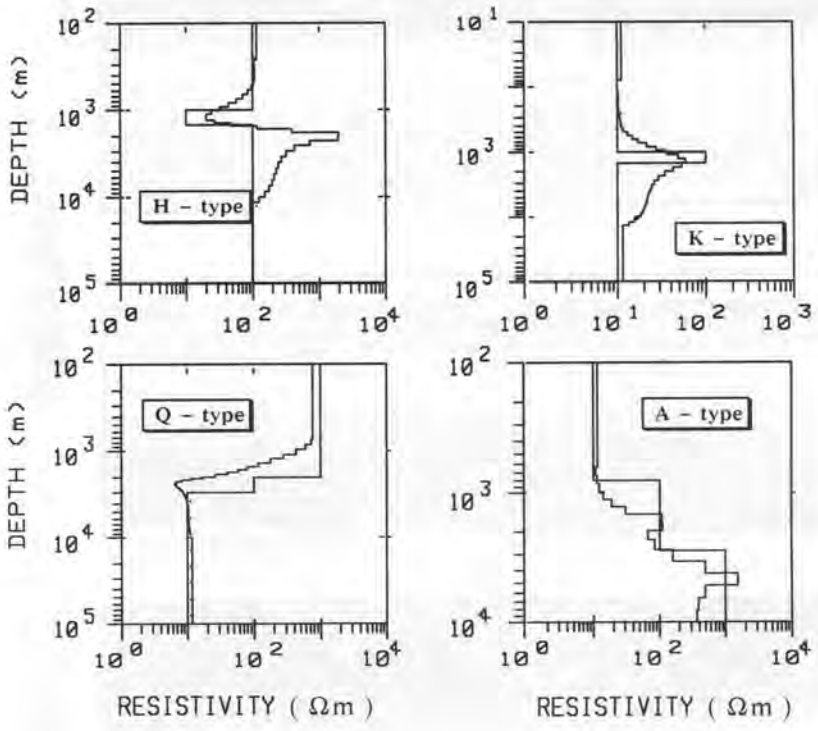

Fig. 2.16: *Source image* for a three-layer model.

For practical applications one needs to know how well the imaging techniques represent structure along a profile. Thus, synthetic data was calculated for a slightly dipping H-type three-layer model simulated with a 1-D layered earth algorithm. This data was then imaged and the results are displayed in figure 2.17 The top of the figure shows the synthetic model in a gray scale representation. The center frame is the

source image and the bottom frame is the *interval resistivity image*. The source image clearly represents the H-type nature of the model and also reflects the dipping of the intermediate layer. The third layer resistivity from the *source image* is higher than the model. This is caused by the typical overshoot in imaging when going to more resistive layers. For the *interval resistivity image*, the gray scale has a smaller range because the *interval resistivity* exhibits less dynamic range. Also, the *interval image* does not clearly reflect the H-type nature of the model. This means that the *source image* preserves more structure of the data than the *interval resistivity image*.

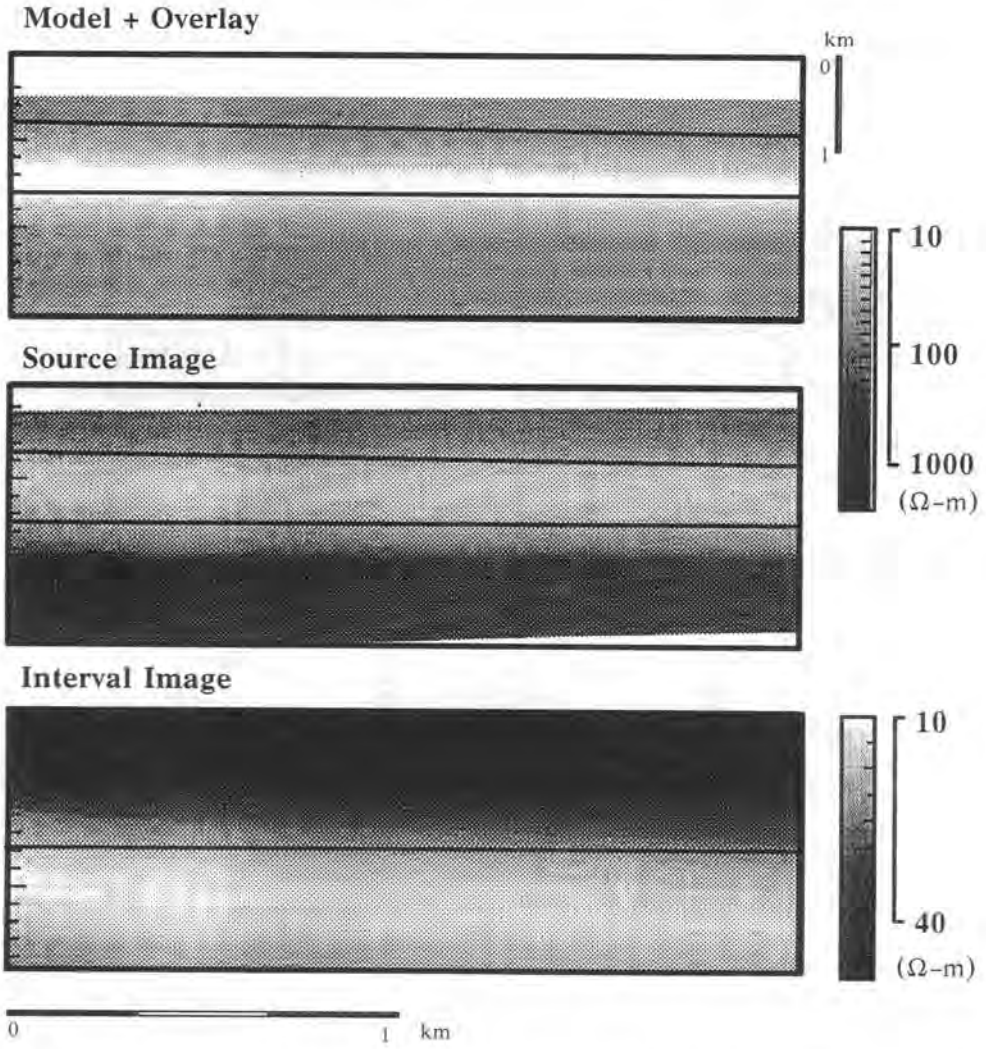

Fig. 2.17: Earth model (top) and the *source imaging* (center) and *interval imaging* (bottom) results.

Since the imaging assumes a 1-D model, namely a layered earth, one must question its applicability to 3-D structures. A typical 3-D effect in LOTEM data are sign reversals (see chapter 4). To illustrate that the source imaging sees a 3-D effect, 3-D synthetic data were calculated for a case history where 1-D and 3-D modeling had to be used to interpret a profile. For this interpretation the reader is referred to chapter 4 and 7 where the respective 1-D and 3-D interpretation is discussed. The 3-D model is shown in figure 2.18. A profile was chosen (A - A') such that is crosses the 3-D anomaly and is close to the station where 3-D effects (sign reversals) were observed.

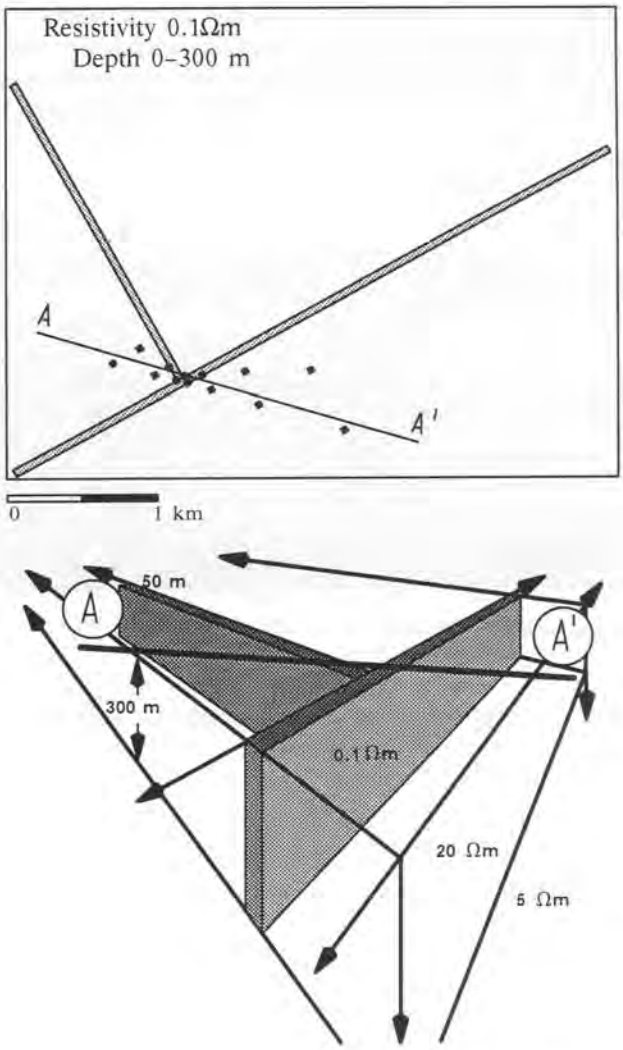

Fig. 2.18: 3-D model and profile location used to calculate the synthetic data for the *source imaging*.

At the same time the profile also contains a part where 1–D interpretation is applicable. The *source image* for this profile is shown in figure 2.19. It clearly exhibits an anomalous area (white part) where the reversals were observed in the field. This means that the source imaging can be used to get a very fast overview where 3–D structures exist.

The above example shows that simple 1–D *source imaging* is a reasonable approach to obtain a fast first interpretation. The computation of the *source image* is so fast, that it can be done in the field within minutes while a full inversion of the same data would take many CPU hours. This is extremely important when considering the increasing amount of data acquired with multichannel systems. Two–dimensional or even three–dimensional imaging or migration would be more appropriate for complex structures, but to date these techniques still require significant interpreter interaction which make the imaging even more time–consuming than standard interpretation (James, 1991).

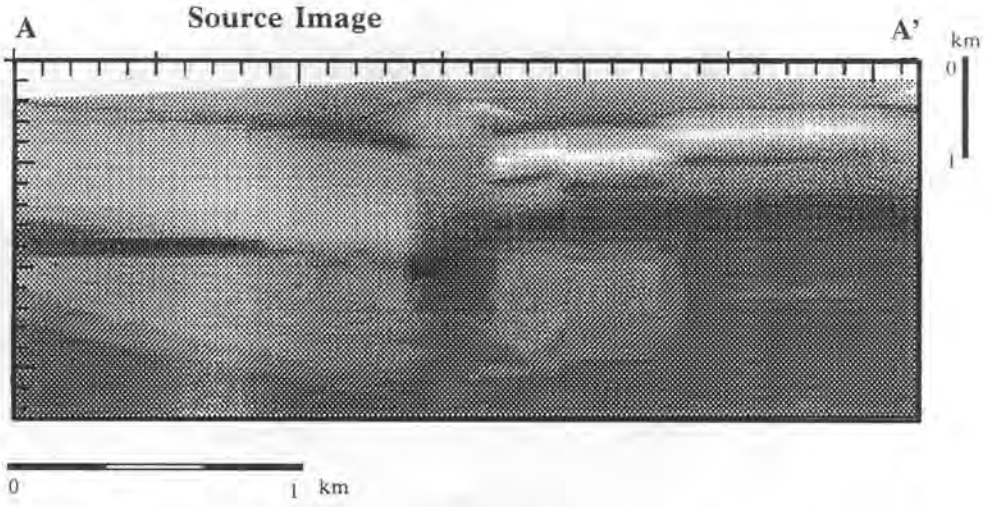

Fig. 2.19: *Source image* of the synthetic data for the 3–D model shown in figure 2.18

KMS Technologies – KJT Enterprises Inc.
6420 Richmond Ave., Suite 610
Houston, Texas, 77057, USA
Tel: 713.532.8144

Please visit us
http://www.kmstechnologies.com